Supplementary Materials for

Nearby Fault Interactions within the Double-Vergence Suture in Eastern Taiwan during the 2022 Chihshang Earthquake Sequence

Chi-Hsien Tang *et al.*

*Yunung Nina Lin. Email: ninalin@earth.sinica.edu.tw

This PDF file includes:

Fig. S1 to S16
Table S1 to S4

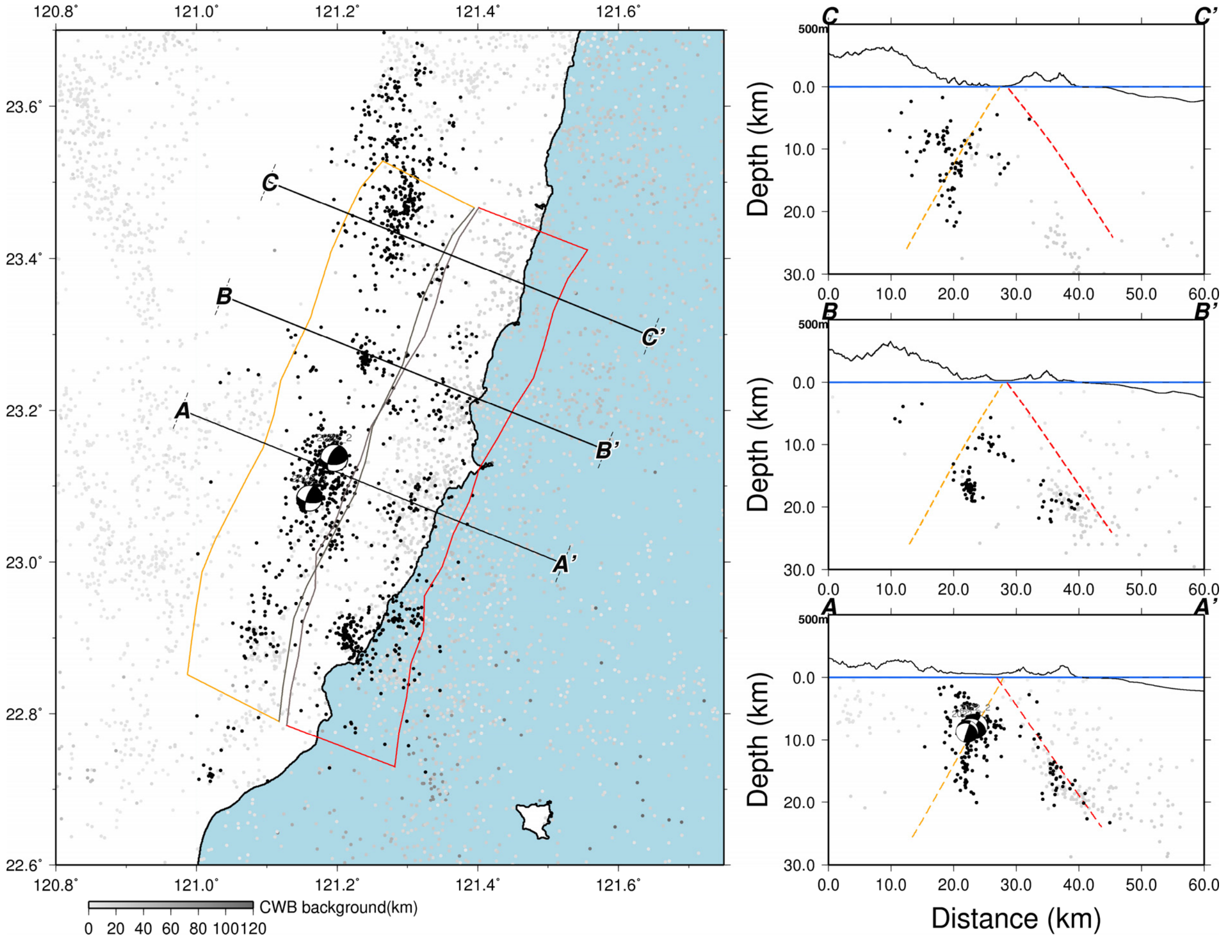

Fig. S1. Background seismicity and aftershocks of the 2022 Chihshang earthquake sequence. Light gray dots: background seismicity between 1990 and 2020[27]. Black dots: relocated aftershocks between September 18 and November 17 (catalog from Taiwan Geophysical Database Management System, Taiwan GDMS, https://gdmsn.cwb.gov.tw/).

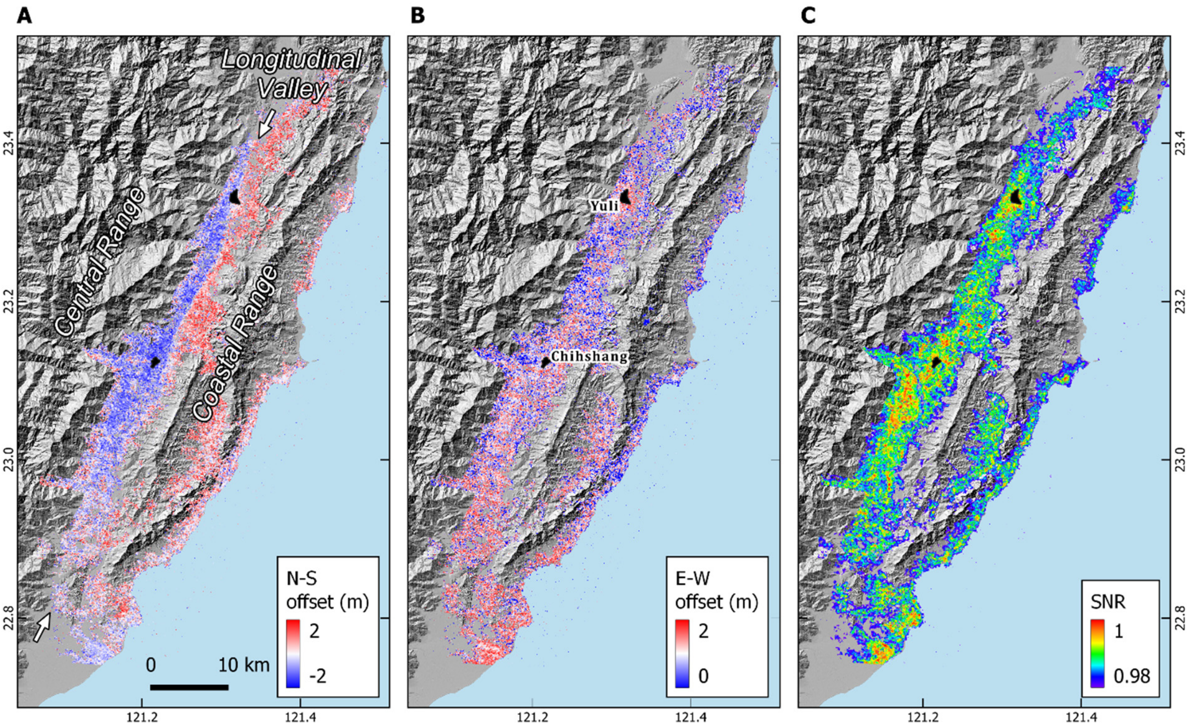

Fig. S2. Pixel offset tracking results from Sentinel-2 images. (**A**) N-S offsets. (**B**) E-W offsets (not used in inversion). (**C**) Signal-to-noise (SNR) ratio. The N-S offsets from Sentinel-2 pixel offset tracking show a sharp boundary in the north and diffused boundary in the south. The E-W offsets, however, do not display any clear trend across the fault because of the rugged topography to the east and west of the Longitudinal Valley.

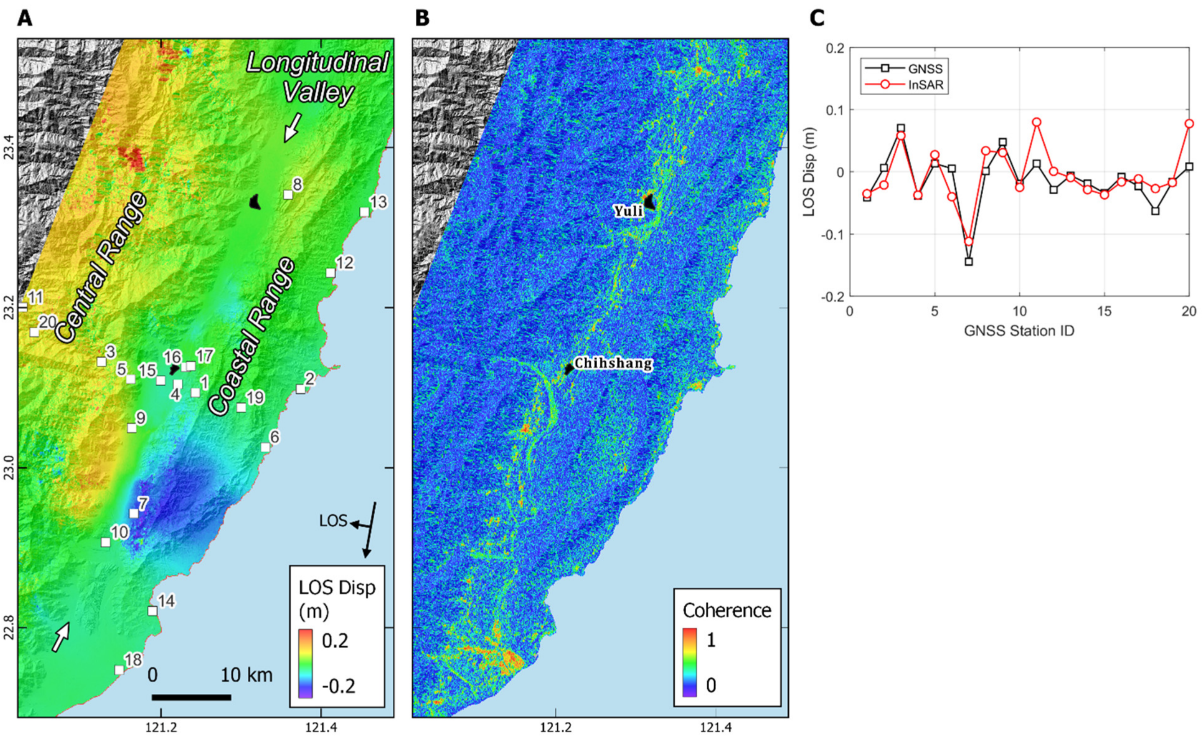

Fig. S3. InSAR results for the foreshock in the 2022 Chihshang earthquake sequence. (**A**) Line-of-sight (LOS) displacement and (**B**) interferometric coherence from ALOS-2 PALSAR-2 ScanSAR images in descending path 27. (**C**) Comparison of coseismic LOS displacements between GNSS and InSAR observations. A static shift is removed from InSAR by calculating the median difference between GNSS and InSAR values. The line-of-sight displacement from InSAR shows good agreement in general with the GNSS coseismic displacements. For stations with larger differences, such as station ID 11 and 20, are located in the Central Range and are more severely affected by low coherence and tropospheric noises.

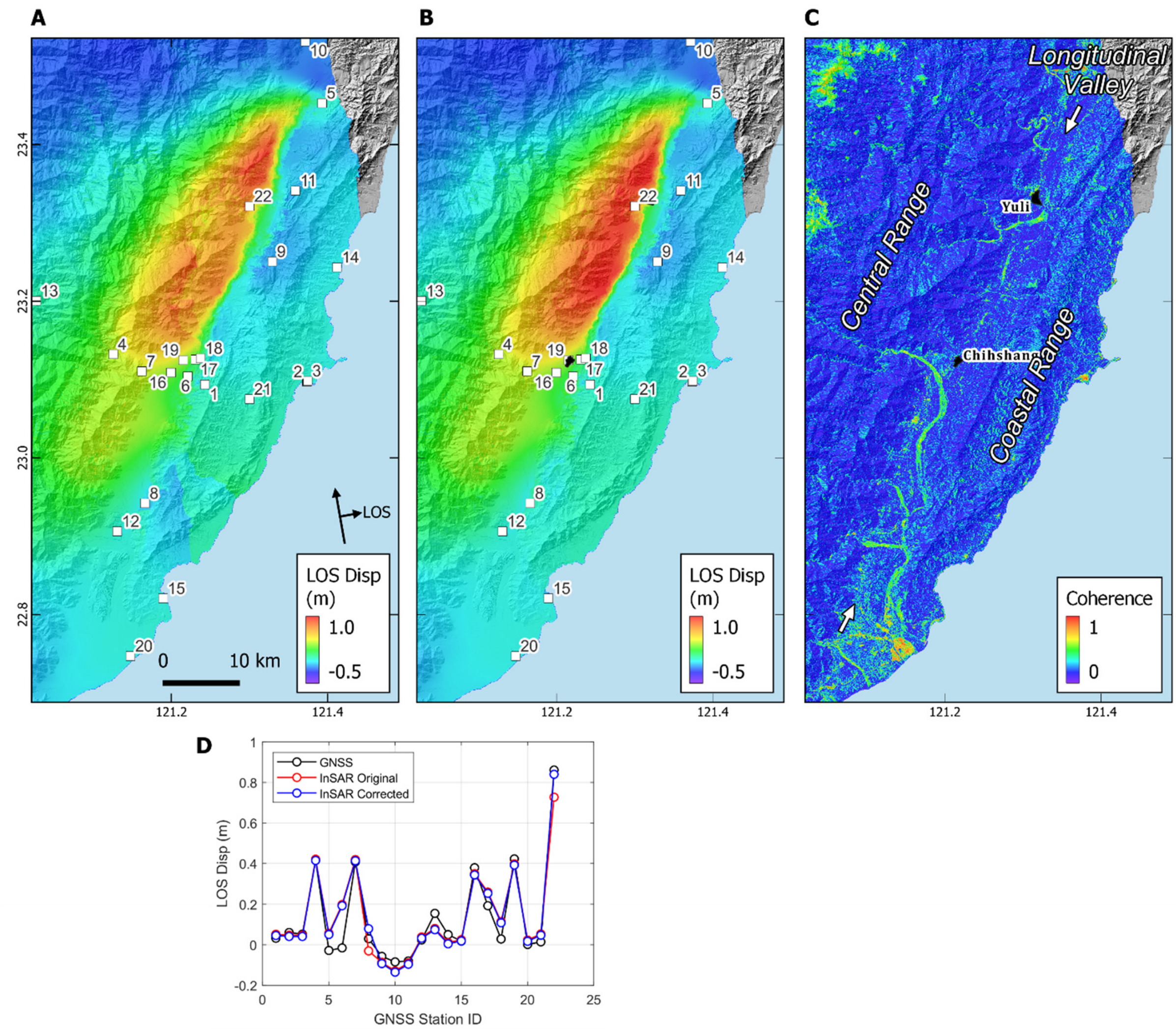

Fig. S4. InSAR results for the mainshock in the 2022 Chihshang earthquake sequence. Line-of-sight (LOS) displacement (**A**) before and (**B**) after manual unwrapping error correction for the interferogram generated from ALOS-2 PALSAR-2 StripMap images in ascending path 137. (**C**) Interferometric coherence. (**D**) Comparison of coseismic LOS displacements between GNSS, the original InSAR (red curve) and the corrected InSAR (blue curve). A static shift is removed from InSAR by calculating the median difference between GNSS and InSAR values. Note the InSAR LOS displacement includes ground deformation for both the foreshock and the mainshock. The discrepancy between InSAR and GNSS observation is significantly reduced in station 8 and 22 after the unwrapping error correction.

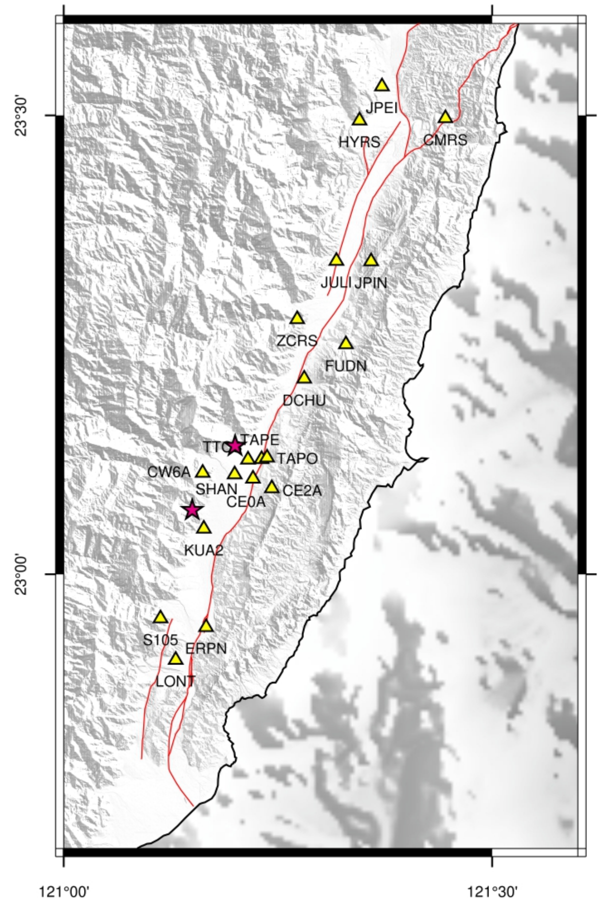

Fig. S5. Location of GNSS stations with 1-Hz position records.

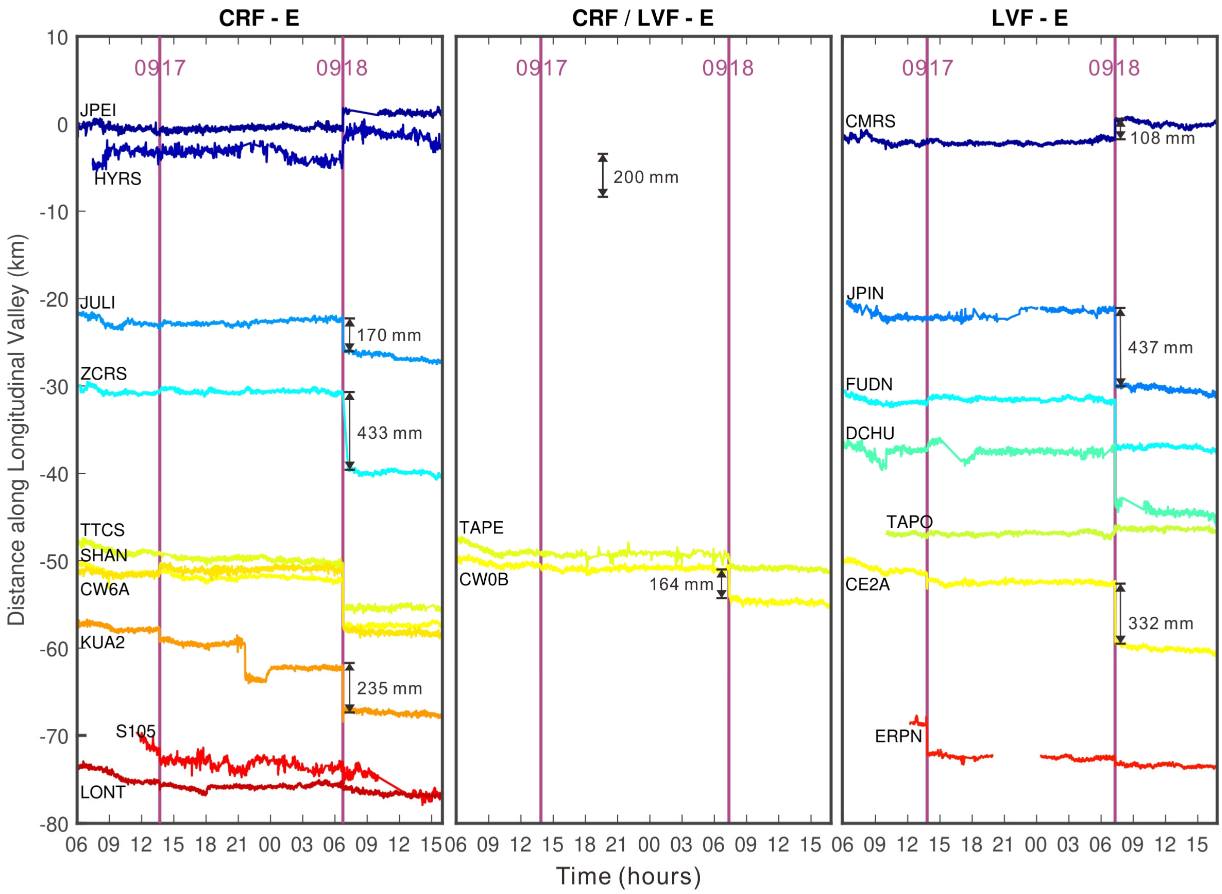

Fig. S6-1. East component of the 1-Hz GNSS position time series. Left panel: stations west of the CRF surface trace. Right panel: stations east of the LVF surface trace. Middle panel: stations in between two faults. Postseismic deformation after the foreshock (0917) can be observed in stations near Chihshang (-50 km in Y-axis). See fig. S4 for station locations.

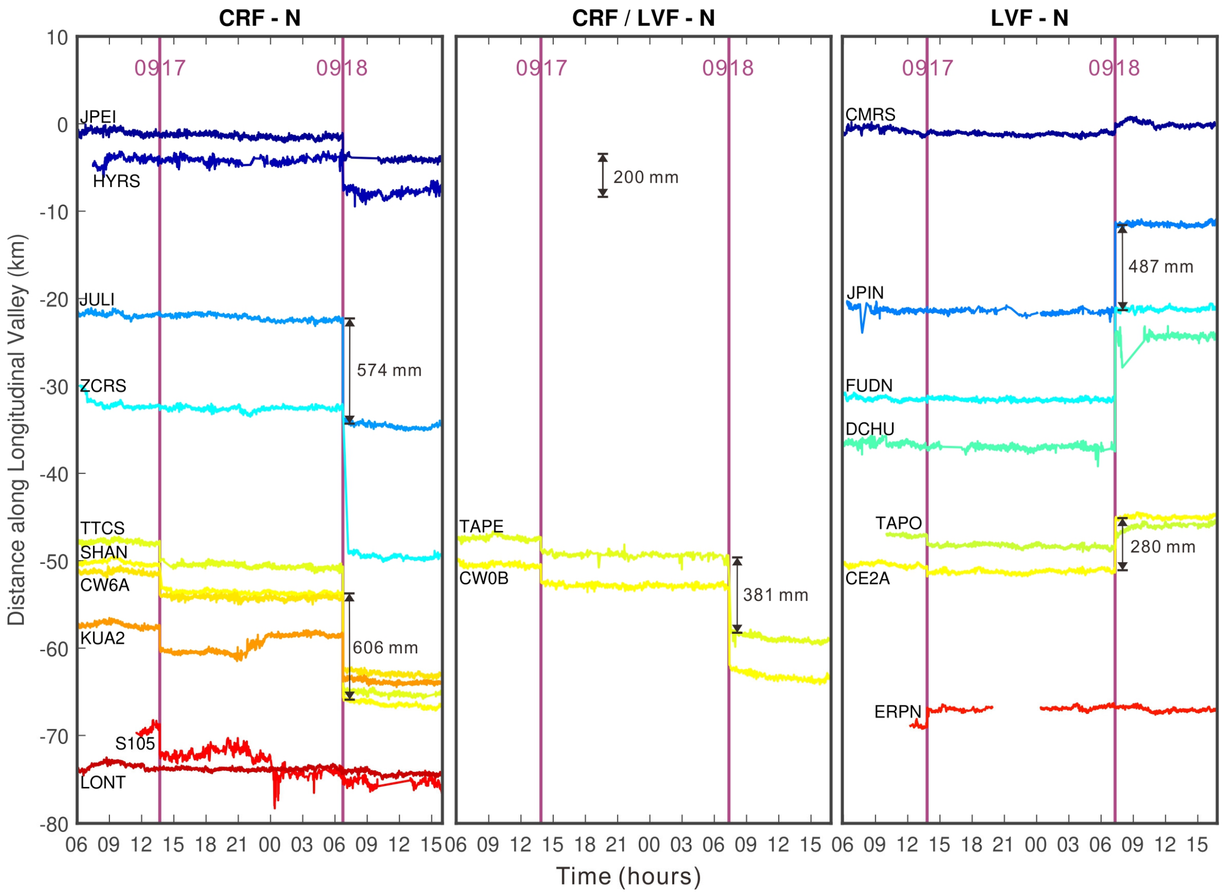

Fig. S6-2. North component of the 1-Hz GNSS position time series. Left panel: stations west of the CRF surface trace. Right panel: stations east of the LVF surface trace. Middle panel: stations in between two faults. Postseismic deformation after the foreshock (0917) can be observed in stations near Chihshang (-50 km in Y-axis). See fig. S4 for station locations.

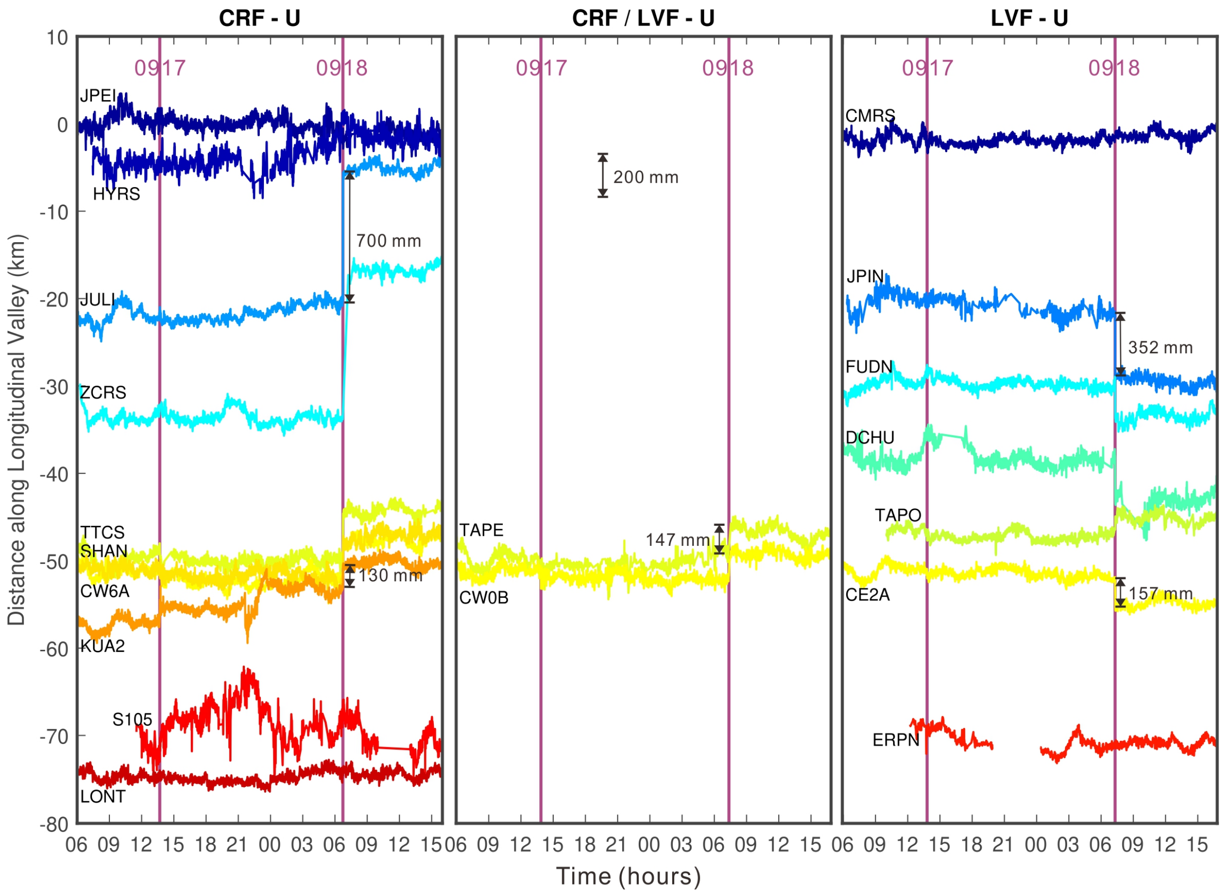

Fig. S6-3. Vertical component of the 1-Hz GNSS position time series. Left panel: stations west of the CRF surface trace. Right panel: stations east of the LVF surface trace. Middle panel: stations in between two faults. See fig. S4 for station locations.

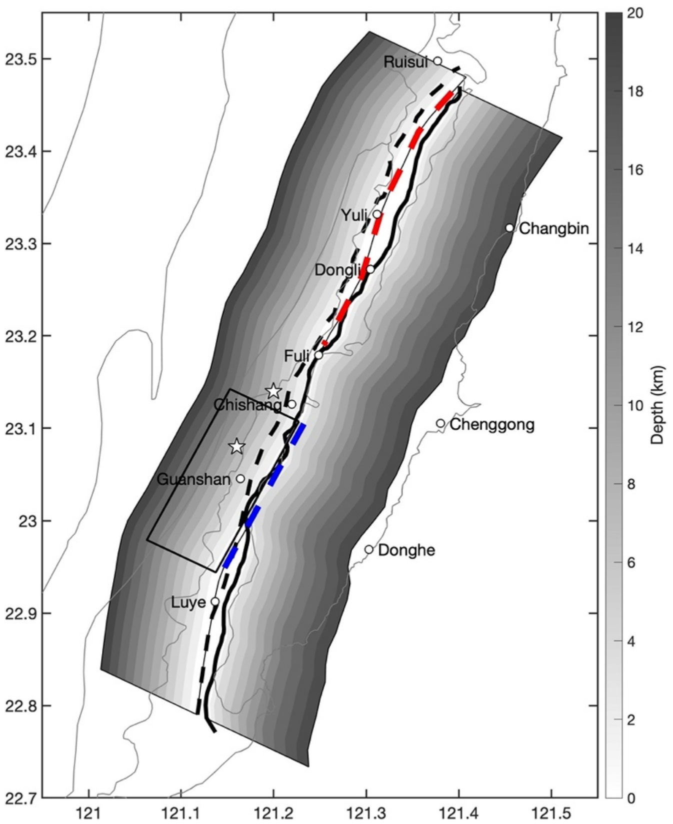

Fig. S7. Fault geometry of the CRF and LVF adopted in this study. Red dashed line shows the coseismic surface rupture along the Yuli fault. Black box area and blue dashed line mark an optimal planar fault and its up-dip surface projection, respectively, for the foreshock. Black dashed and solid lines are the CRF and LVF in the TEM model[28].

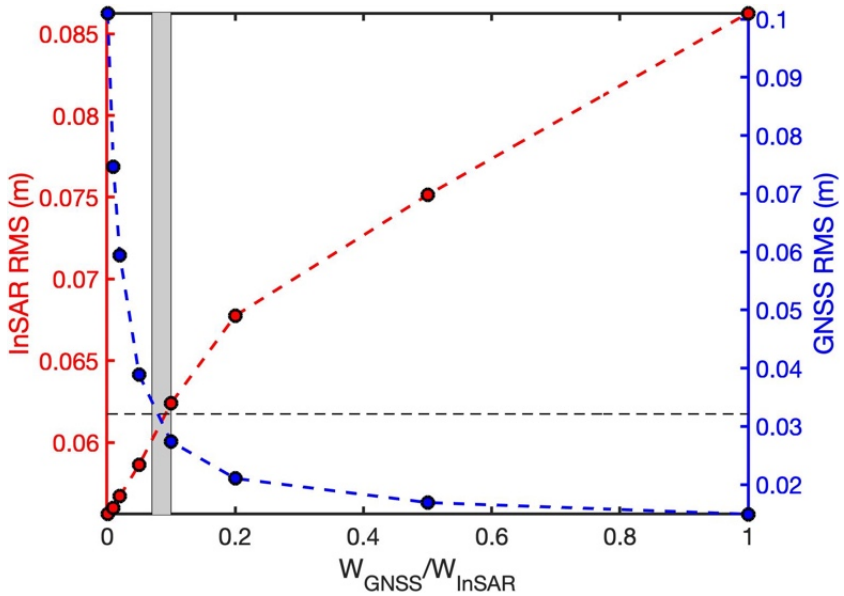

Fig. S8. Root-mean-square (RMS) of the InSAR and GNSS data as a function of their relative weight in the joint inversion. Red and blue curves show InSAR and GNSS data, respectively. Black dashed line represents 20% of the RMS between the minimum and maximum values in the diagram. Gray-shaded area shows the plausible range of the relative weight to balance the fit of both InSAR and GNSS data.

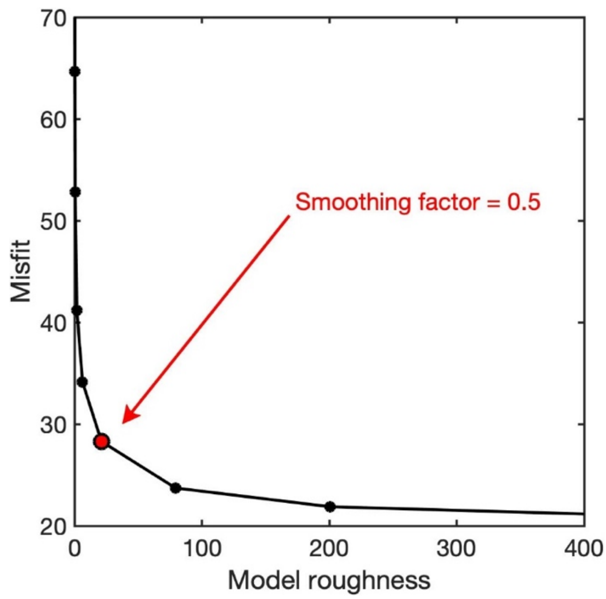

Fig. S9. L-curve between the misfit and the model roughness for the coseismic slip model. Red dot is the smoothing factor adopted in this study.

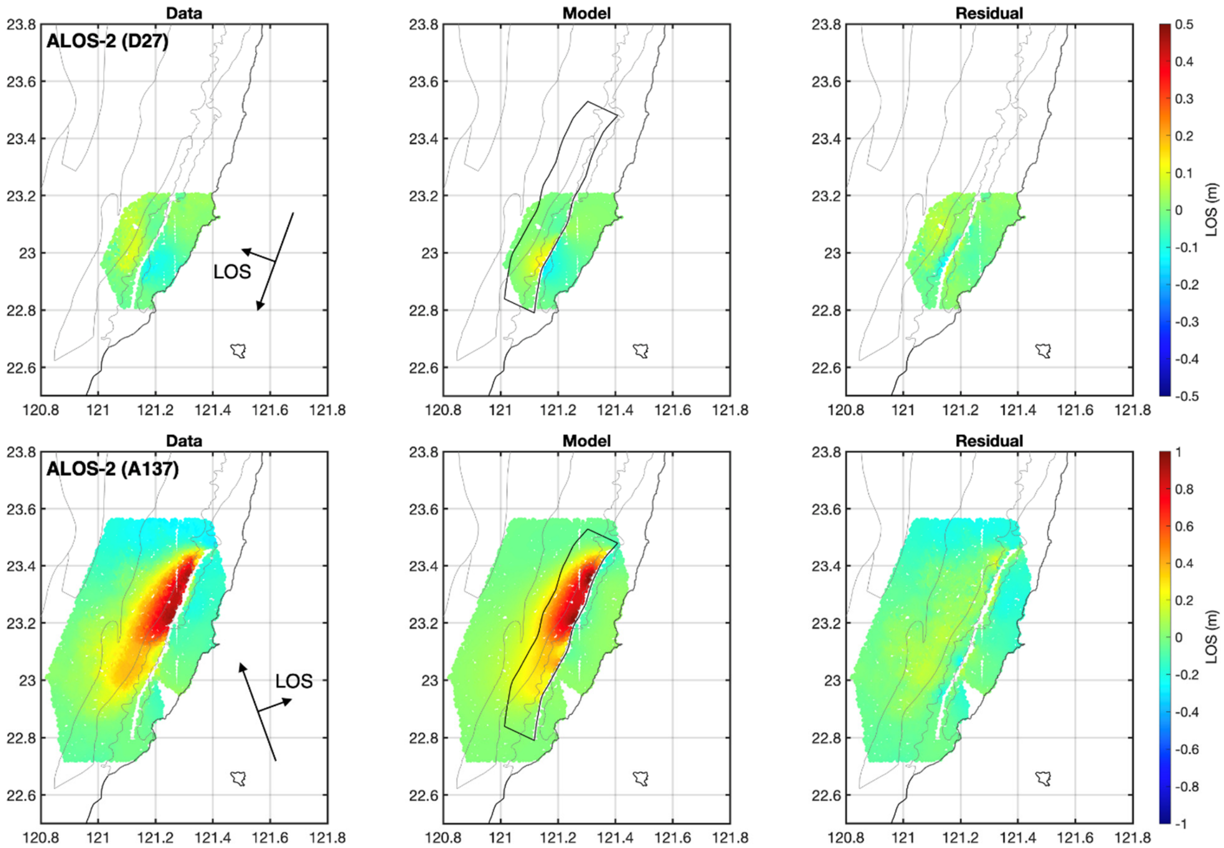

Fig. S10-1. Observed, modeled and residual InSAR LOS displacements (CRF for both the foreshock and the mainshock). Panels from left to right show data, model, and residual, respectively. Black lines outline the geometry of the CRF and LVF. Note the color scales for D27 and A137 are different. See Table S1 for RMSE reports.

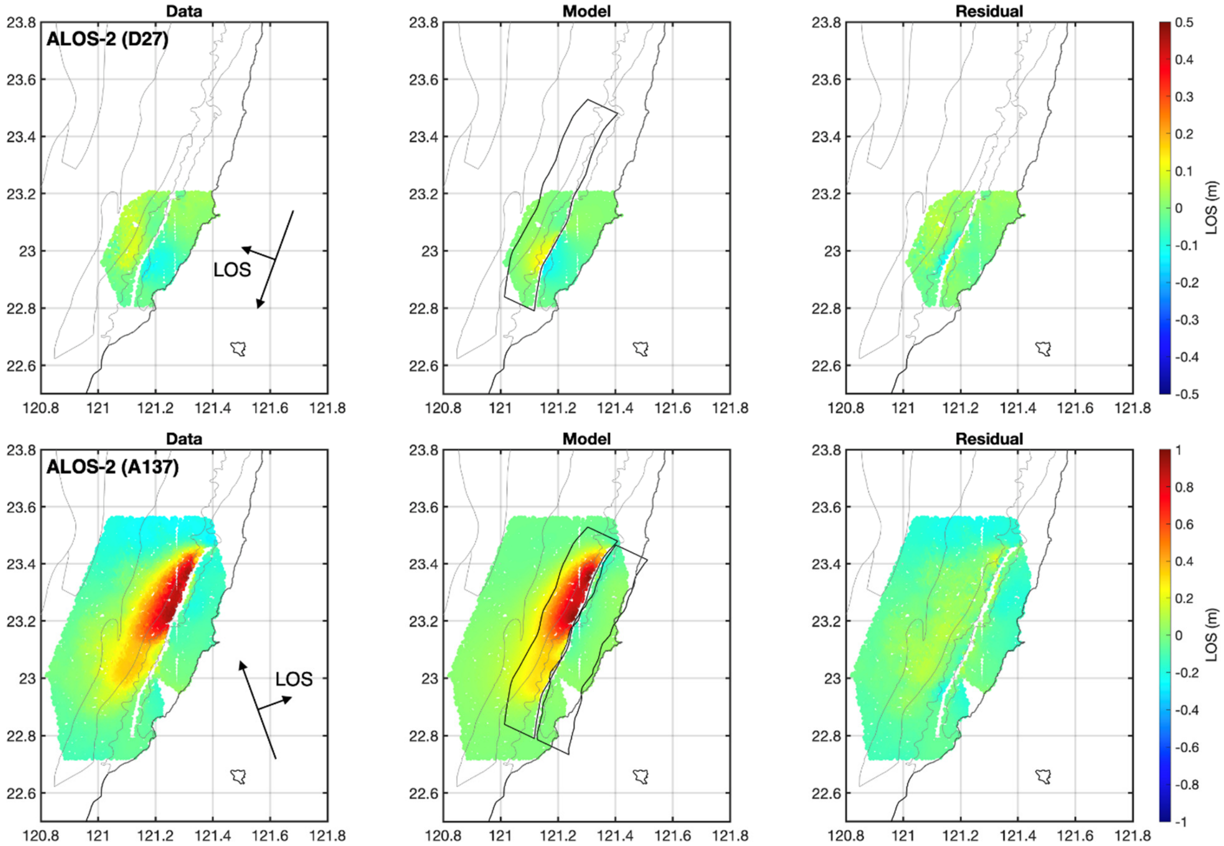

Fig. S10-2. Observed, modeled and residual InSAR LOS displacements (CRF for the foreshock and CRF+LVF for the mainshock). Panels from left to right show data, model, and residual, respectively. Black lines outline the geometry of the CRF and LVF. Note the color scales for D27 and A137 are different. See Table S1 for RMSE reports.

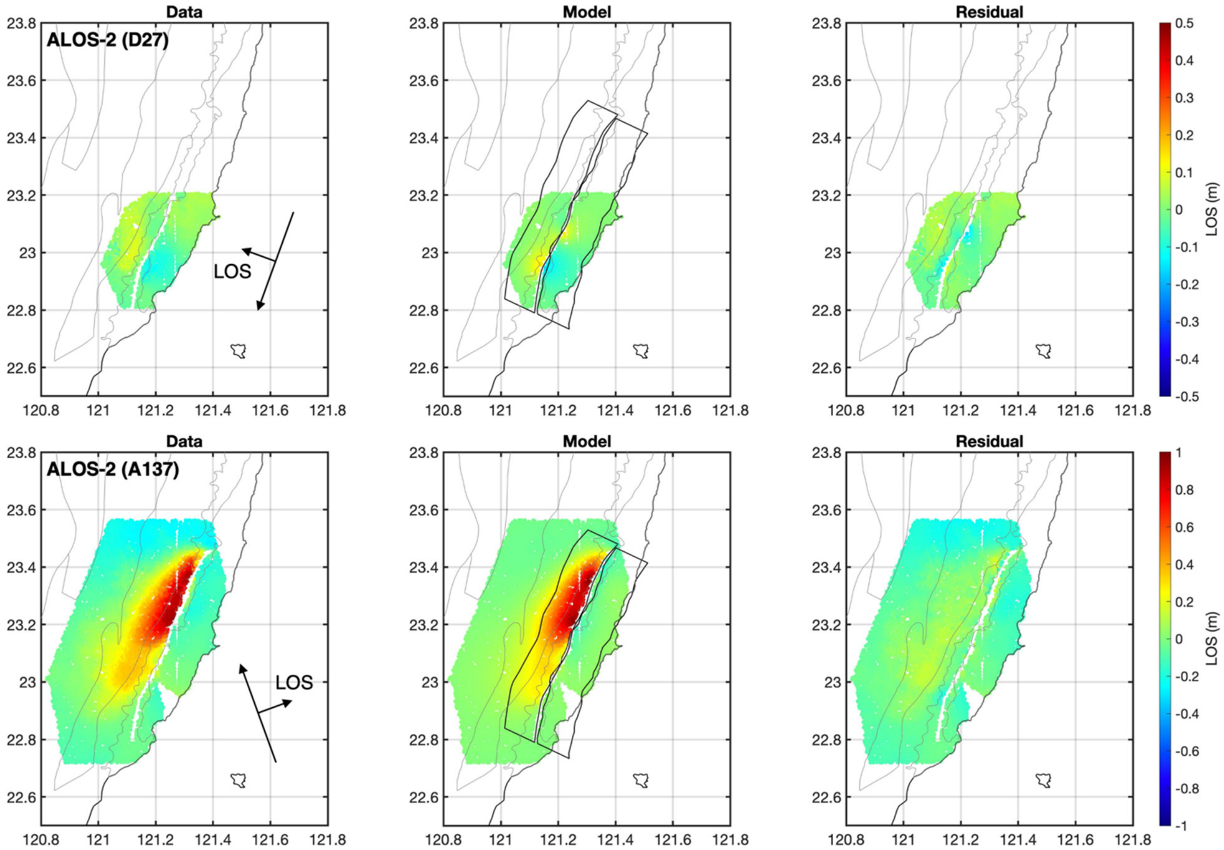

Fig. S10-3. Observed, modeled and residual InSAR LOS displacements (CRF+LVF for both the foreshock and the mainshock). Panels from left to right show data, model, and residual, respectively. Black lines outline the geometry of the CRF and LVF. Note the color scales for D27 and A137 are different. See Table S1 for RMSE reports.

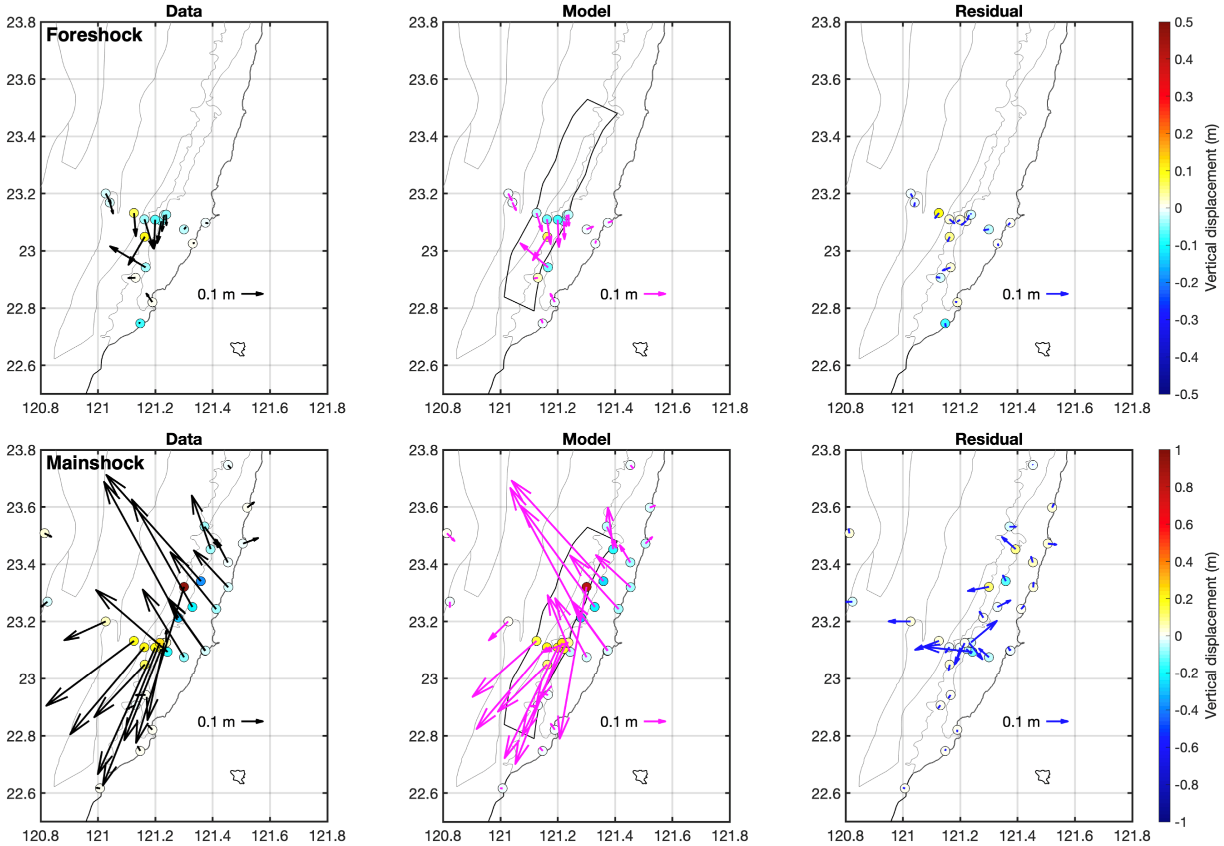

Fig. S11-1. Observed, modeled and residual GNSS static coseismic displacements (CRF for both the foreshock and the mainshock). Panels from left to right show data, model, and residual, respectively. Black lines outline the geometry of the CRF and LVF. Note the color scales for vertical displacements during the foreshock and mainshock are different. See Table S1 for RMSE reports.

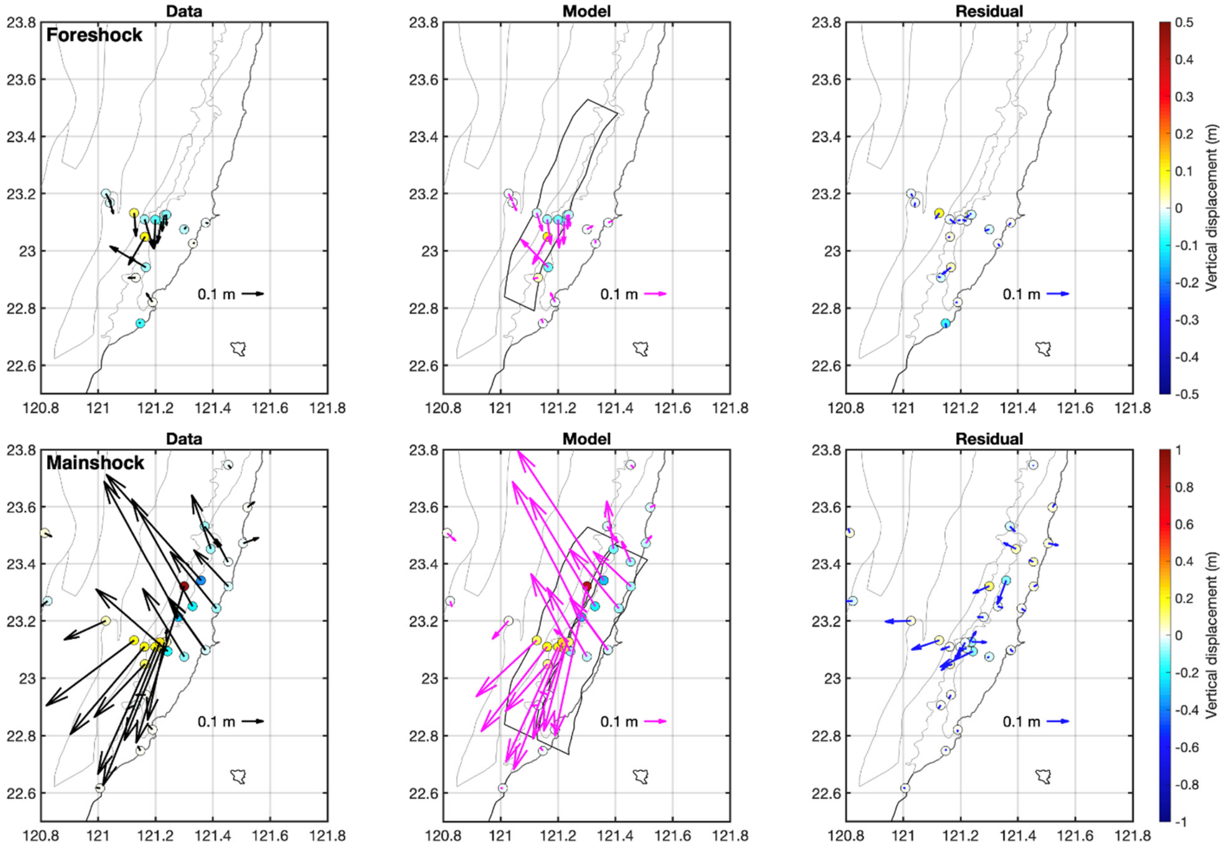

Fig. S11-2. Observed, modeled and residual GNSS static coseismic displacements (CRF for the foreshock and CRF+LVF for the mainshock). Panels from left to right show data, model, and residual, respectively. Black lines outline the geometry of the CRF and LVF. Note the color scales for vertical displacements during the foreshock and mainshock are different. See Table S1 for RMSE reports.

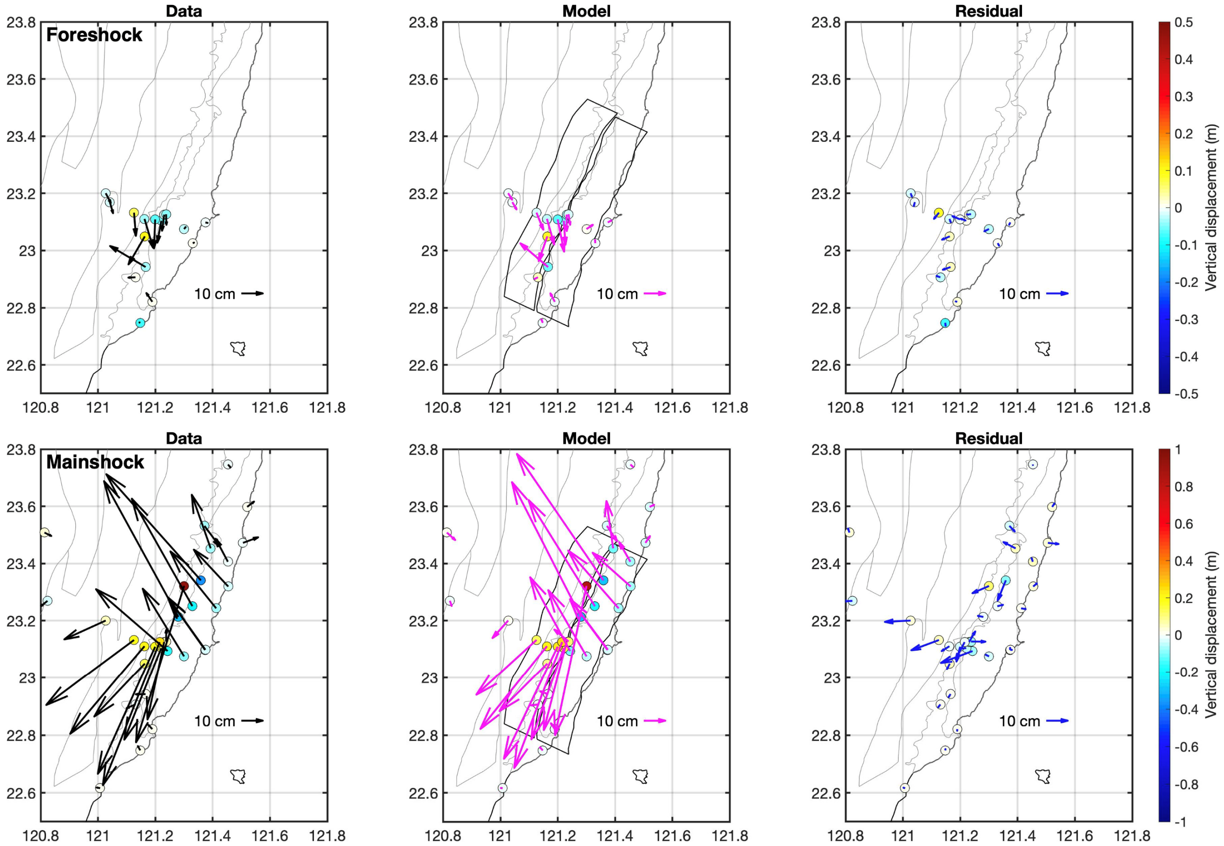

Fig. S11-3. Observed, modeled and residual GNSS static coseismic displacements (CRF+LVF for both the foreshock and the mainshock). Panels from left to right show data, model, and residual, respectively. Black lines outline the geometry of the CRF and LVF. Note the color scales for vertical displacements during the foreshock and mainshock are different. See Table S1 for RMSE reports.

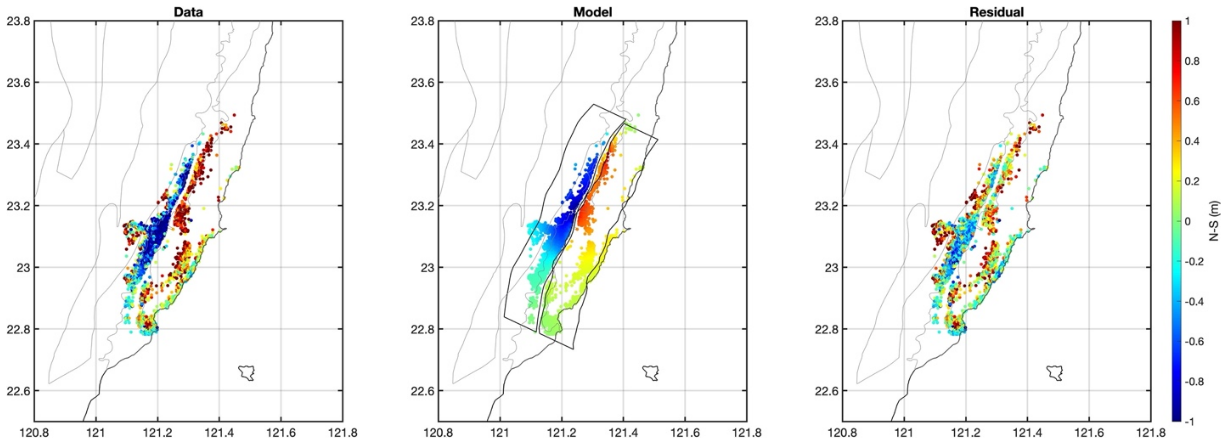

Fig. S12. Observed, modeled and residual N-S pixel offsets from Sentinel-2 optical images (CRF for the foreshock and CRF+LVF for the mainshock). Panels from left to right show data, model, and residual, respectively. Black polygons outline the geometry of the CRF and LVF. Note the large noise in the data. This dataset is not included in scenario testing due to lower signal-to-noise ratios.

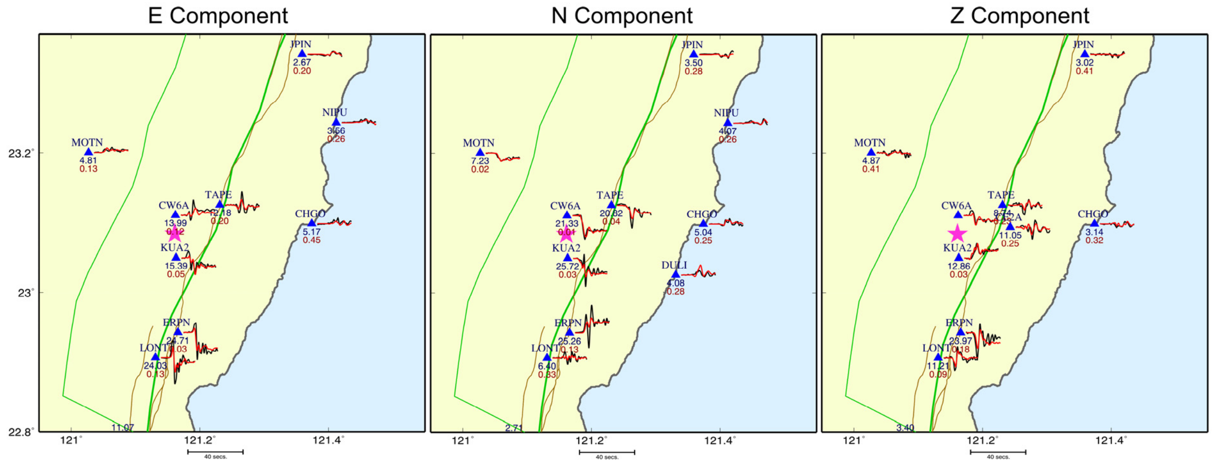

Fig. S13-1. Observed and modeled HR-GNSS records for the foreshock (CRF only). Data and model are shown in black and red, respectively. Green and orange polygons represent the CRF and the LVF respectively. Numbers under each station indicate the maximum amplitude (blue in cm) and misfit of waveform (red), respectively. See Table S2 for RMSE reports.

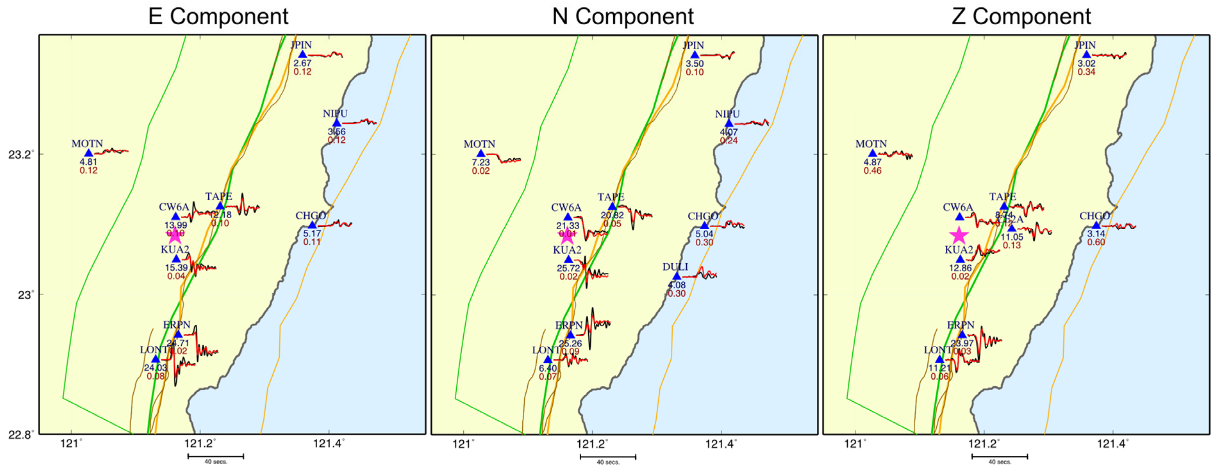

Fig. S13-2. Observed and modeled HR-GNSS records for the foreshock (CRF+LVF). Data and model are shown in black and red, respectively. Green and orange polygons represent the CRF and the LVF respectively. Numbers under each station indicate the maximum amplitude (blue in cm) and misfit of waveform (red), respectively. See Table S2 for RMSE reports.

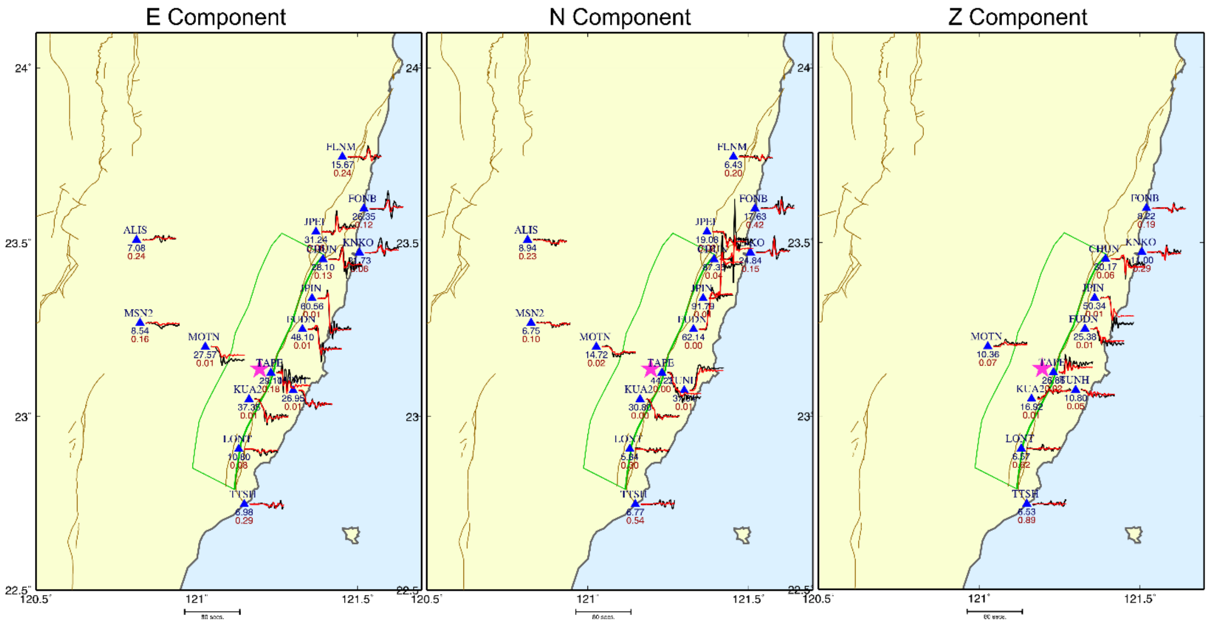

Fig. S14-1. Observed and modeled HR-GNSS records for the mainshock (CRF only). Data and model are shown in black and red, respectively. Green and orange polygons represent the CRF. Numbers under each station indicate the maximum amplitude (blue in cm) and misfit of waveform (red), respectively. Brown curves are the latest version of active faults published by the Central Geological Survey[59]. See Table S2 for RMSE reports.

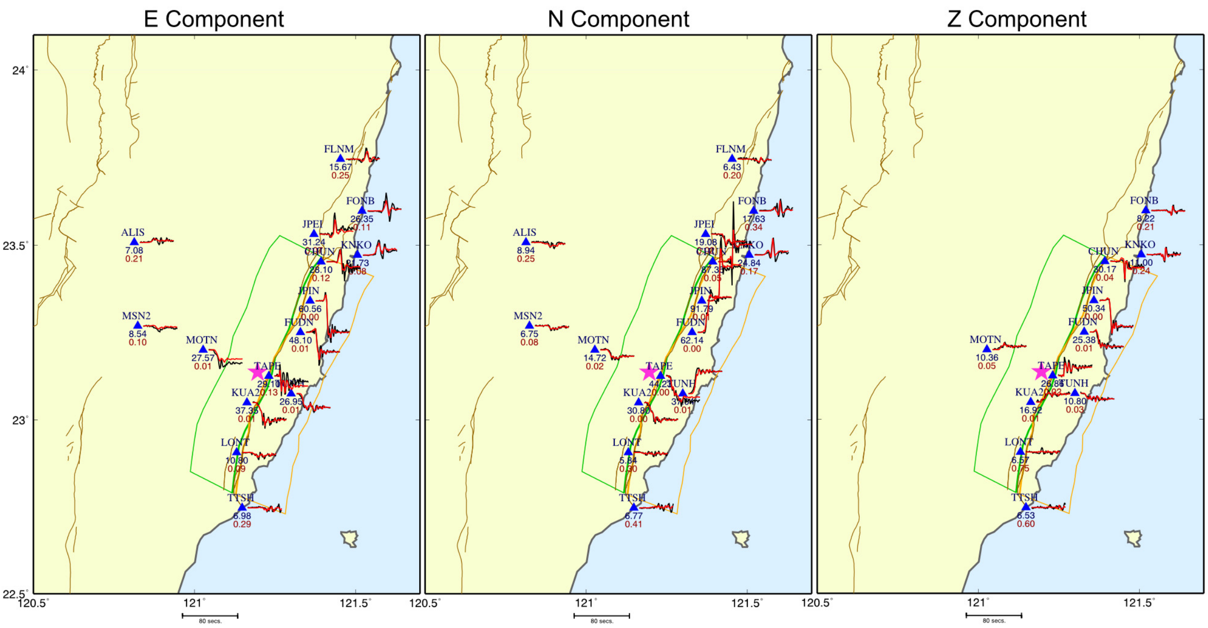

Fig. S14-2. Observed and modeled HR-GNSS records for the mainshock (CRF+LVF). Data and model are shown in black and red, respectively. Green and orange polygons represent the CRF and the LVF respectively. Numbers under each station indicate the maximum amplitude (blue in cm) and misfit of waveform (red), respectively. Brown curves are the latest version of active faults published by the Central Geological Survey[59]. See Table S2 for RMSE reports.

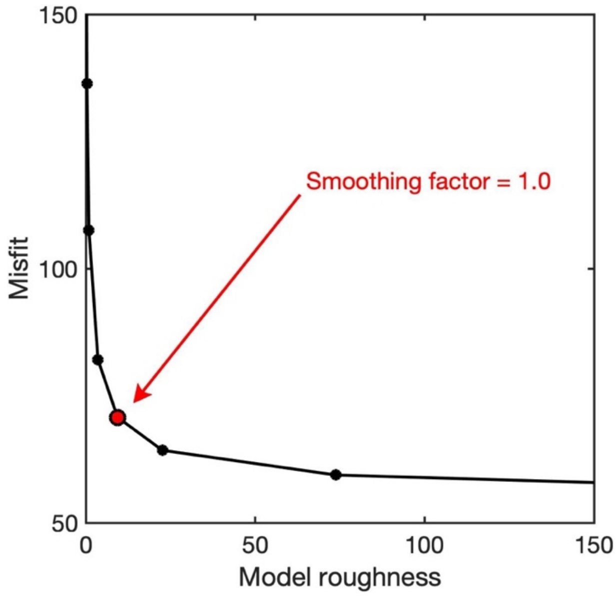

Fig. S15. L-curve between the misfit and the model roughness for the 34-day afterslip model. Red dot marks the adopted smoothing factor.

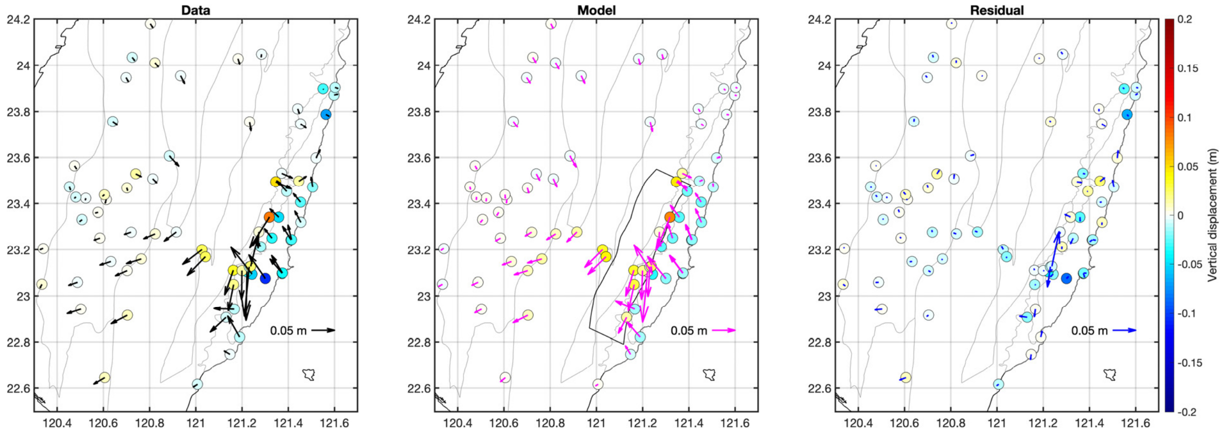

Fig. S16-1. Observed, modeled and residual GNSS 34-day postseismic displacements (CRF only). Panels from left to right show data, model, and residual, respectively. Black lines outline the geometry of the CRF and LVF. See Table S3 for RMSE reports.

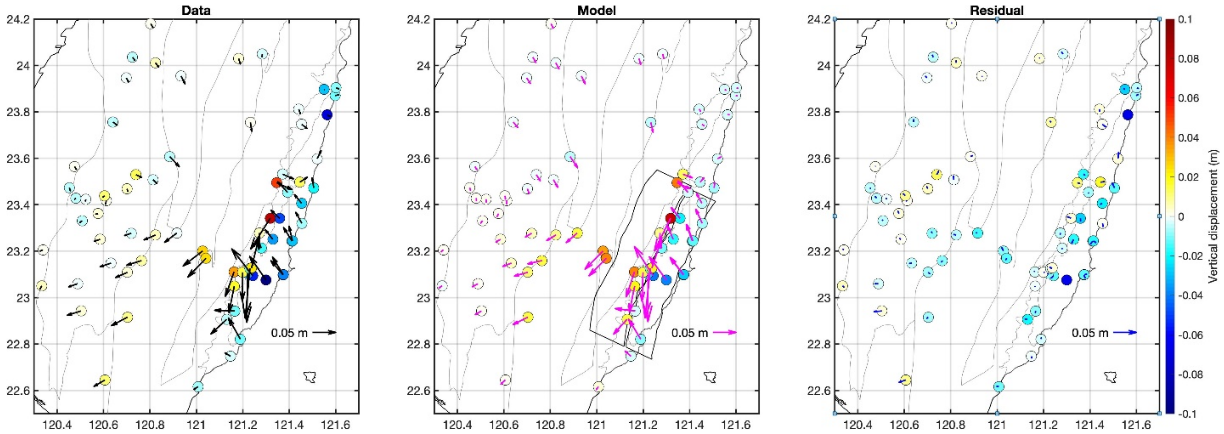

Fig. S16-2. Observed, modeled and residual GNSS 34-day postseismic displacements (CRF+LVF). Panels from left to right show data, model, and residual, respectively. Black lines outline the geometry of the CRF and LVF. See Table S3 for RMSE reports.

Table S1. RMSE (in cm) for coseismic displacement data fitting in different model scenarios

	Model Scenario (Foreshock +Mainshock Joint Inversion)*			
	Foreshock Fault Plane	**CRF**	**CRF**	**CRF+LVF**
	Mainshock Fault Plane	**CRF**	**CRF+LVF**	**CRF+LVF**
GNSS				
Foreshock displacements		2.4	2.2	2.5
Mainshock displacements		4.1	3.5	3.5
InSAR				
D27 (foreshock only)		2.7	2.7	2.7
A137 (foreshock + mainshock)		8.4	7.0	6.9

*All four sets of data are jointed fitted in the same inversion within each model scenario. The number of faults may vary between the foreshock and the mainshock (the second scenario). See *Co-seismic and postseismic slip inversion* in the *Method* section.

Table S2. RMSE (in cm) for HR-GNSS data fitting in different model scenarios

	Model Scenario	
	CRF	**CRF+LVF**
Foreshock 1-Hz position time series	2.6	2.3
Mainshock 1-Hz position time series	4.4	3.2

Table S3. RMSE (in cm) for postseismic data fitting in different model scenarios

	Model Scenario	
	CRF	**CRF+LVF**
1-month postseismic displacements	1.2	0.9

Table S4. Parameters used in moment budget estimation

	CRF	LVF
Fault Setup		
full length (km)	140	140
full width (km)	30	30
dip (deg)	55[a]	35-70[a]
average rake (deg)	45	45
Geologic Rates		
dip slip rate (mm/yr)	4.8-7.8[b]	20.5-26.9[c,d]
full slip rate (mm/yr)*	6.7-11.0	29.0-38.0
Shallow Creeping		
length (km)		60[e]
width (km)		5[f]
rate (mm/yr)		33[e,f]
Stress Shadow Effect		
source event	1951 EQ	2022 EQ
length (km)	140	60
width (km)	30	30

[a]Maximum dip angle in ref[28]

[b]Derived by using the terrace uplift rates in ref[20] and the dip angle of 55 deg

[c]ref[43]

[d]ref[60]

[e]ref[37]

[f]ref[35]

*Given the average rake